# A Hybrid Electrochemical/Chemical Synthesis of Zinc Oxide Nanoparticles and Optically Intrinsic Thin Films

Ralph M. Nyffenegger,† Ben Craft, Mohammed Shaaban, Sasha Gorer, Georg Erley, and Reginald M. Penner*

*Department of Chemistry, Institute for Surface and Interface Science, University of California−Irvine, Irvine, California 92697-2025*

*Received November 3, 1997. Revised Manuscript Received January 27, 1998*

A hybrid electrochemical/chemical (E/C) synthesis of zinc oxide (ZnO) nanoparticles and films is described. The E/C procedure involves two steps: Zinc metal was first electrochemically deposited at basal-plane oriented graphite electrode surfaces from dilute aqueous solutions; then this deposit was permitted to spontaneously oxidize and dehydrate at open circuit in the pH = 1.0 plating solution. Deposition was size-selective, and wurtzite phase ZnO nanocrystallites having mean diameters in the range from 15 to 100 Å were obtained using this approach. Relative standard deviations of the particle diameter for ZnO particle dispersions varied from 25 to 50%. Polycrystalline ZnO films of 100−400 Å in thickness were also obtained by depositing larger quantities of zinc metal in the first step of the synthesis. For ZnO particles (dia. < 80 Å), electron diffraction analysis revealed a preferred orientation for ZnO crystallites where the *c*-axis of the wurtzite unit cell was oriented perpendicular to the plane of the graphite surface, but X-ray powder diffraction data indicated that this orientational preference was lost when larger quantities of zinc were deposited and ZnO films were obtained. Luminescence spectra for the ZnO films prepared using this E/C method consisted of a single exciton band near 3.2 eV at room temperature with no deep trap state emission. At low temperatures (20 K), this exciton band split into a cleanly resolved and fully assignable phonon loss progression.

## I. Introduction

Zinc oxide (ZnO) is a large band gap ($E_G$ = 3.2 eV) n-type semiconductor that possesses optical properties which render it important industrially as a phosphor in field emissive displays[1,2] and in other cathodoluminescent devices,[3] as a photocatalyst (e.g., for the oxidation of hydrocarbons[4]), and as the gain medium in UV semiconductor lasers.[5] A wide variety of synthetic methods have been employed to prepare ZnO colloids and films, some of which are sol−gel chemistry,[6−11] spray pyrolysis,[12] metal−organic chemical vapor deposition (MOCVD),[13−16] and cathodic electrodeposition.[17−19] Despite the technological importance of ZnO as an optical material and the quantity of literature devoted to its study (more than 600 scientific papers since 1989), it has so far proven to be impossible to prepare "optically intrinsic" ZnO thin films or nanoparticles—defined here as material that exhibits *no trap state emission* in its luminescence spectrum.

Specifically, ZnO prepared using any of the methods listed above exhibits a broad luminescence peak with a maximum anywhere in the range 1.95−2.75 eV (450−635 nm), i.e., at an energy well below that of the band gap of 3.2 eV. This "green" emission, which has been known for at least 65 years,[20] has been attributed to the inclusion of trace amounts of dopant species during synthesis: species such as $Cl^-$, $Br^-$,[21] $Cu^{2+}$,[22] $Li^+$,[23,24] $Al^{3+}$, $Ga^{3+}$,[21] and trivalent rare earths ($Ho^{3+}$, $Dy^{3+}$, $Gd^{3+}$, and $Sm^{3+}$).[3,21,25,26] A competing hypothesis is that these trap states derive from native defects including

* Address correspondence to this author at rmpenner@uci.edu.
† Current address: Park Scientific Instruments Inc., Sunnyvale, CA.

(1) Vanheusden, K.; Seager, C. H.; Warren, W. L.; Tallant, D. R.; Voight, J. A. *J. Appl. Phys.* **1996**, *68*, 403.
(2) Vanheusden, K.; Warren, W. L.; Seager, C. H.; Tallant, D. R.; Voight, J. A. *J. Appl. Phys.* **1996**, *79*, 7983.
(3) Bachir, S.; Sandouly, C.; Kossanyi, J.; Ronfard-Haret, J. C. *J. Phys. Chem. Solids* **1996**, *57*, 1869−79.
(4) Pichat, P.; Herrmann, J.-M.; Disdier, J.; Mozzanega, M.-N. *J. Phys. Chem.* **1979**, *83*, 3122.
(5) Kurbatov, L. N.; Kozina, G. S.; Kostinskaya, T. A.; Rudnevskii, V. S.; Lobachev, A. N.; Kuznetsov, V. A.; Kuz'mina, I. P.; Shaldin, Y. V.; Shternberg, A. A. *Kvantovaya Elektronika, Moskva* **1980**, *7*, 378−82.
(6) Hoyer, P.; Eichenberger, R.; Weller, H. *Ber. Bunsen.-Ges. Phys. Chem.* **1993**, *97*, 630.
(7) Hoyer, P.; Weller, H. *Chem. Phys. Lett.* **1994**, *221*, 379−84.
(8) Bahnemann, D. W.; Kormann, C.; Hoffmann, M. R. *J. Phys. Chem.* **1987**, *91*, 3789−3798.
(9) Haase, M.; Weller, H.; Henglein, A. *J. Phys. Chem.* **1988**, *92*, 482.
(10) Sakohara, S.; Tickanen, L. D.; Anderson, M. A. *J. Phys. Chem.* **1992**, *96*, 11086−91.
(11) Spanhel, L.; Anderson, M. A. *J. Am. Chem. Soc.* **1991**, *113*, 2826−2833.
(12) De Merchant, J.; Cocivera, M. *Chem. Mater.* **1995**, *7*, 1742.
(13) Roth, A. P.; Williams, D. F. *J. Appl. Phys.* **1981**, *52*, 6685−92.
(14) Roth, A. P.; Williams, D. F. *J. Electrochem. Soc.* **1981**, *128*, 2684−6.
(15) Maruyama, T.; Shionoya, J. *J. Mater. Sci. Lett.* **1992**, *11*, 170−2.
(16) Bethke, S.; Pan, H.; Wessels, B. W. *Appl. Phys. Lett.* **1988**, *52*, 138−40.
(17) Izaki, M.; Omi, T. *Appl. Phys. Lett.* **1996**, *68*, 2439−40.
(18) Izaki, M.; Omi, T. *J. Electrochem. Soc.* **1996**, *143*, L53−5.
(19) Peulon, S.; Lincot, D. *Adv. Mater.* **1996**, *8*, 166−70.
(20) Bancroft, W. D.; Gurchot, C. *J. Phys. Chem.* **1932**, *36*, 2575.
(21) Kroger, F. A.; Vink, H. J. *J. Chem. Phys.* **1954**, *22*, 250.

S0897-4756(97)00718-7 CCC: $15.00 
Published on Web 03/19/1998

**Scheme 1**

**A. "Direct"Electrochemical Synthesis.**

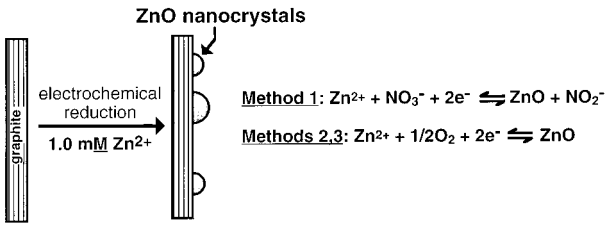


**B. Electrochemical/Chemical Synthesis.**

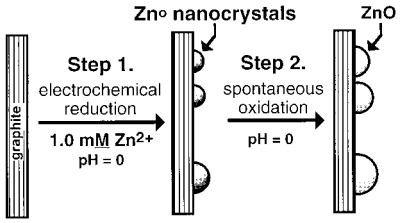


ionized zinc interstitials (electron traps) coupled with zinc vacancies (hole traps),[27,28] oxygen vacancies,[29] and (recently) singly ionized oxygen vacancies.[2] Depending on the particular synthetic method which has been employed, a second narrower emission peak at an energy corresponding to the band gap (3.2 eV or 387 nm) is sometimes seen in addition to the trap state emission. However the trap state emission has been ubiquitous at room temperature with the ratio, $R_{295}$, defined here as the intensity of the trap state peak to that of the near band edge (NBE) emission at room temperature,[30] exceeding 0.10 in all previous experiments with more typical values for $R_{295}$ in the range 0.5−20.

Here, we describe a hybrid electrochemical/chemical (or E/C) method for synthesizing supported ZnO films on graphite surfaces which are optically intrinsic ($R_{295}$ < 0.01). We further demonstrate that this E/C method can be employed to prepare ZnO nanoparticles in a size-selective fashion, but the optical characterization of these particles is not reported in this paper. Unlike previous electrochemical syntheses of ZnO[17−19] in which particles or films were obtained in a single cathodic deposition step (e.g., Scheme 1A), the E/C procedure (Scheme 1B) involves two steps: The electrochemical deposition of zinc nanocrystals (or thin films) onto a graphite basal plane surface, and the spontaneous oxidation (yielding $Zn(OH)_2$) and dehydration of the zinc deposit to yield wurtzite phase ZnO. Although this procedure is simple and straightforward, it enables the size-selective preparation of ZnO nanoparticles over the range of mean diameters from 15 to 100 Å, and it can also be employed to produce nanocrystalline films of ZnO up to 400 Å in thickness on HOPG surfaces. The luminescence spectroscopy of such films show the lowest levels of trap state emission ever seen for ZnO films or particles. The synthesis procedure described here is derived from the E/C method we have recently employed for the preparation of graphite-supported nanocrystals of copper(I) iodide[31] and cadmium sulfide.[32] In fact, the first two steps of the E/C syntheses of CuI and CdS are exactly analogous to the ZnO synthesis reported here.

## II. Materials and Methods

**II.A. Methods of ZnO Sample Preparation.** In addition to the synthesis of ZnO via the E/C method, we have prepared ZnO films and particles using three other *"direct" electrochemical methods* for purposes of comparison: *method 1*—a chloride and oxygen free solution of 50 mM $ZnNO_3$, in 0.10 M $KNO_3$ with a deposition potential of − 0.7 V vs NHE. This procedure is one of several investigated by Izaki and Omi.[17,18] Another direct electrochemical method is *method 2*—an $O_2$-saturated solution of 1.0 mM $ZnCl_2$, 0.1 M KCl with a deposition potential of 0.040 V vs NHE at 295 K. These parameters are within the ranges specified by Peulon and Lincot[19] in their study. The final method is *method 3*—an $O_2$-saturated solution of 1.0 mM $Zn(ClO_4)_2$, 0.1 M $HClO_4$ with a deposition potential of 0.040 V vs NHE (a chloride-free variant of the Peulon and Lincot method). Following deposition, samples were removed from the electrochemical cell, rinsed with water, and air-dried. Deposition durations are specified below. All of these solutions were prepared using as received reagent grade chemicals. The effect of thermal annealing of these deposits (at 250−400 °C in air for 30 min) was also investigated.

*"E/C" ZnO.* "E/C" ZnO deposition involved the potentiostatic deposition of zinc metal at −1.1 V vs NHE, and the spontaneous oxidation of these particles at open circuit in the plating solution for a few seconds. Thermal annealing of this deposit (at 250−400 °C in air for 30 min) did not further improve its crystallinity or modify its optical properties, but this step was sometimes carried out to rapidly dry the deposit following synthesis and prior to characterization. Zinc deposition pulse durations varied from milliseconds to 30 s (vide infra). The plating solution was prepared by dissolving zinc powder (99.998%, Aldrich) in $HClO_4$ (trace metal grade by Fischer); the ultimate $HClO_4$ concentration was 1.0 M. This solution was $N_2$-sparged prior to use.

*ZnO Powder.* In addition, a ZnO powder was synthesized as follows: $Zn(OH)_2$ powder was precipitated by increasing the pH of aqueous, 1.0 mM $ZnClO_4$ via the dropwise addition of NaOH to this solution. The dehydration and annealing of this powder at 250−400 °C in air for 30 min yielded wurtzite phase ZnO powder. This ZnO powder was used as a structural standard in electron diffraction investigations.

All aqueous solutions were prepared using Barnsted Nanopure water ($\rho \geq 18$ MΩ cm). Coulometry could not be used as a reliable indicator of the quantity of ZnO deposited in any of these experiments because the deposition of ZnO always occurred in conjunction with a second reaction: either the evolution of $H_2$ or the reduction of dissolved $O_2$. The contribution of these secondary reactions to the total charge could not

(22) Dingle, R. *Phys. Rev. Lett.* **1969**, *23*, 579−81.
(23) Georgobiani, A. N.; Butkhuzi, T. V.; Khulordava, T. G.; El'tazarov, B. T. *Sbornik Kratkie Soobshcheniya po Fizike, AN SSSR, Fizicheskii Institut im. P. N. Lebedeva* **1984**, 46−9.
(24) Georgobiani, A. N.; Butkhuzi, T. V.; Alexsandrov, O. V.; Khulordava, T. G. *Sbornik Kratkie Soobshcheniya po Fizike, AN SSSR, Fizicheskii Institut im. P. N. Lebedeva* **1984**, 50−3.
(25) Bachir, S.; Kossanyi, J.; Ronfard-Haret, J. C. *Solid State Comm.* **1994**, *89*, 859−63.
(26) Bachir, S.; Kossanyi, J.; Sandouly, C.; Valat, P.; Ronfard-Haret, J. C. *J. Phys. Chem.* **1995**, *99*, 5674.
(27) Bylander, E. G. *J. Appl. Phys.* **1978**, *49*, 1188−95.
(28) Takata, S.; Minami, T.; Nanto, H.; Kawamura, T. *Phys. Status Solidi* **1981**, K83.
(29) Anpo, M.; Kubokawa, Y. *J. Phys. Chem.* **1984**, *88*, 5556−60.
(30) The intensity of the trap state emission relative to that of the NBE emssion intensity (i.e., *R*) decreases dramatically as the temperature is decreased from 295 K to cryogenic temperatures.
(31) Hsiao, G. S.; Anderson, M. G.; Gorer, S.; Harris, D.; Penner, R. M. *J. Am. Chem. Soc.* **1997**, *119*, 1439−1448.
(32) Anderson, M. A.; Gorer, S.; Penner, R. M. *J. Phys. Chem. B* **1997**, *101*, 5895.

readily be estimated (and subtracted) because ZnO particles served to catalyze both of these reactions to an appreciable extent.

**II.B. Noncontact Atomic Force Microscopy.** Noncontact AFM experiments in air were performed using a commercial instrument (Park Scientific Instruments (PSI Inc.) AutoProbe CP). Cantilevers were 2.0 $\mu$m thick Ultralevers (PSI Inc.) having a force constant of 18 N/m, a resonance frequency near 300 kHz, and a nominal tip radius of 100 Å. The cantilever excitation frequency employed for these measurements was adjusted to be near the maximum slope of the cantilever resonance response curve. A free-space amplitude of cantilever motion (far from the surface) of ~100 Å was employed, and the cantilever amplitude was damped to ~30 Å during imaging. The piezo tube employed for these investigations was calibrated in the direction perpendicular to the surface using graphite basal plane surfaces on which monatomic steps were introduced by heating in flowing $O_2$ in a tube furnace at 650 °C for 2−3 min. Lateral calibration of the piezo tube was performed by atomic resolution imaging of HOPG and Au(111). Following electrochemical deposition of ZnO on a graphite surface, the surface was removed from the plating solution, rinsed briefly in a stream of Nanopure water, dried at 60 °C, and imaged in air. Statistical analysis of the images was performed using NIH Image (the National Institute of Health).

**II.C. Transmission Electron Microscopy, Selected Area Electron Diffraction, and X-ray Diffraction.** Transmission electron microscopy (TEM) and selected area electron diffraction data were acquired on ZnO nanocrystallites and thin films without removing the ZnO from the graphite basal plane surface. A proven method for accomplishing this analysis[31−33] is by preparing a working electrode consisting of thin (100−400 Å thick) HOPG flakes (~1 mm$^2$) supported on carbon-coated gold TEM grids (Ted Pella). The electrochemical deposition of ZnO was then performed on this electrode using one of the procedures described above. TEM data were obtained on a Philips EM-200 microscope using an accelerating voltage of 200 keV. Diffraction patterns were obtained at a camera length of 1000 mm using a selected area aperture having a diameter of 10 $\mu$m.

X-ray powder diffraction data (XRD) data was acquired using a Mo source having $\lambda = 0.7093$ Å. ZnO thin films appropriate for XRD analysis were deposited onto conductive tin-doped indium oxide (ITO) coated glass slides instead of graphite because HOPG diffractions interfered with important zinc oxide lines.

**II.D. Luminescence Spectroscopy.** Laser-induced luminescence spectra were acquired as previously described[31,32] using 50−200 mW continuous wave excitation from an argon ion laser at 351 nm. Briefly, laser light with p-polarization was incident on the sample at Brewster's angle (~60°) from surface normal. Emission was collected at normal incidence through a 20× Zeiss EpiPlan microscope objective, n.a. = 0.4. The light was then coupled with an f4 lens into an imaging spectrograph (Chromex 250IS, equipped with a 1200 grove mm$^{-1}$ and 300 grove mm$^{-1}$ holographic grating; both 500 nm blaze) which dispersed the light onto a liquid-nitrogen-cooled CCD (Princeton Instruments Model LN/1024EUV) having 1024 × 256 pixels. Signal from the 256 pixels arrayed perpendicular to long axis of the CCD were binned producing a linear detector with 1024 channels. The pixel-wise resolution of this detector was 0.6 and 2.3 meV using the 1200 and 300 grove mm$^{-1}$ gratings, respectively. The sample was contained in a cryostat cooled with a closed cycle helium refrigerator which permitted control of the sample temperature from ambient down to 20° K. Collection times varied between 0.05 and 30 s.

## III. Results and Discussion

**III.A. ZnO Prepared by Direct Deposition.** We have looked here at the properties of the existing electrochemical methods for depositing ZnO particles and films in order to assess the properties of these methods for obtaining particles and films on HOPG surfaces and to evaluate for the first time the photoluminescence from cathodically deposited ZnO.

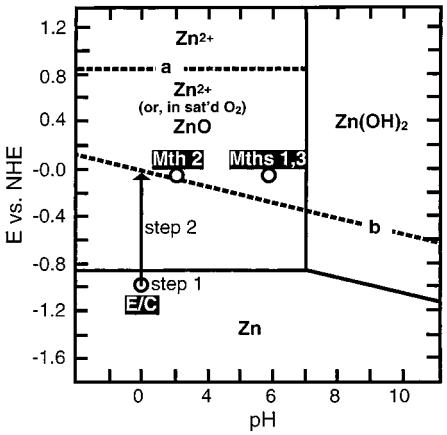


**Figure 1.** Pourbaix diagram for $[Zn^{2+}] = 1.0$ mM indicating the synthesis conditions employed for the preparation of ZnO by the various methods investigated in this study. The line labeled "a" delineates the reaction $Zn^{2+} + {}^1/_2O_2 + 2e^- \leftrightarrows ZnO$ having an $E° = 0.888$ V vs NHE. The region below this line is either a region of stability for $Zn^{2+}$ (in the absence of dissolved $O_2$) or a region of stability for ZnO (in a solution saturated with $O_2$); the line labeled "b" delineates the reaction $2H^+ + 2e^- \leftrightarrows H_2$.

Previously, the "direct" electrodeposition of ZnO onto ITO glass substrates has been accomplished using two different methods. Izaki and Omi[17,18] showed that ZnO can be cathodically deposited from aqueous, $N_2$-sparged zinc nitrate solutions at potentials of −0.7 V vs Ag/AgCl, possibly according to the mechanism:

$$H_2O + NO_3^- + 2e^- \leftrightarrows NO_2^- + 2OH^- \quad (E° = 0.01 \text{ V vs NHE}) \quad (1)$$

$$Zn^{2+} + 2OH^- \leftrightarrows Zn(OH)_2 \quad (2)$$

$$Zn(OH)_2 \leftrightarrows ZnO + H_2O \quad (3)$$

$$Zn^{2+} + NO_3^- + 2e^- \leftrightarrows ZnO + NO_2^- \quad (4)$$

The oxygen source in this case is the nitrate anion, and the Pourbaix diagram (Figure 1) does not apply in the presence of nitrate because of the existence of this ZnO deposition route. In our analogue of this procedure (method 1), we have employed 50 mM $ZnNO_3$—a concentration which yielded stoichiometric ZnO at close to the maximum deposition rate (on ITO glass) of 0.015 $\mu$m min$^{-1}$ (or 2.5 Å s$^{-1}$) in that work.

Peulon and Lincot[19] cathodically deposited zinc oxide films from aqueous $O_2$-containing zinc chloride solutions according to the net reaction:

$$Zn^{2+} + {}^1/_2O_2 + 2e^- \leftrightarrows ZnO \quad (E° = 0.88 \text{ V vs NHE}) \quad (5)$$

In that work, ZnO was obtained for a wide range of deposition potentials ranging from 0.80 V vs NHE (i.e., the Nernst potential of reaction 2), to the onset of the reduction of $Zn^{2+}$ to zinc metal ($E = -0.76$ V vs NHE)

(33) Zoval, J. V.; Lee, J.; Gorer, S. A.; Penner, R. M. *J. Phys. Chem.*, submitted for publication.

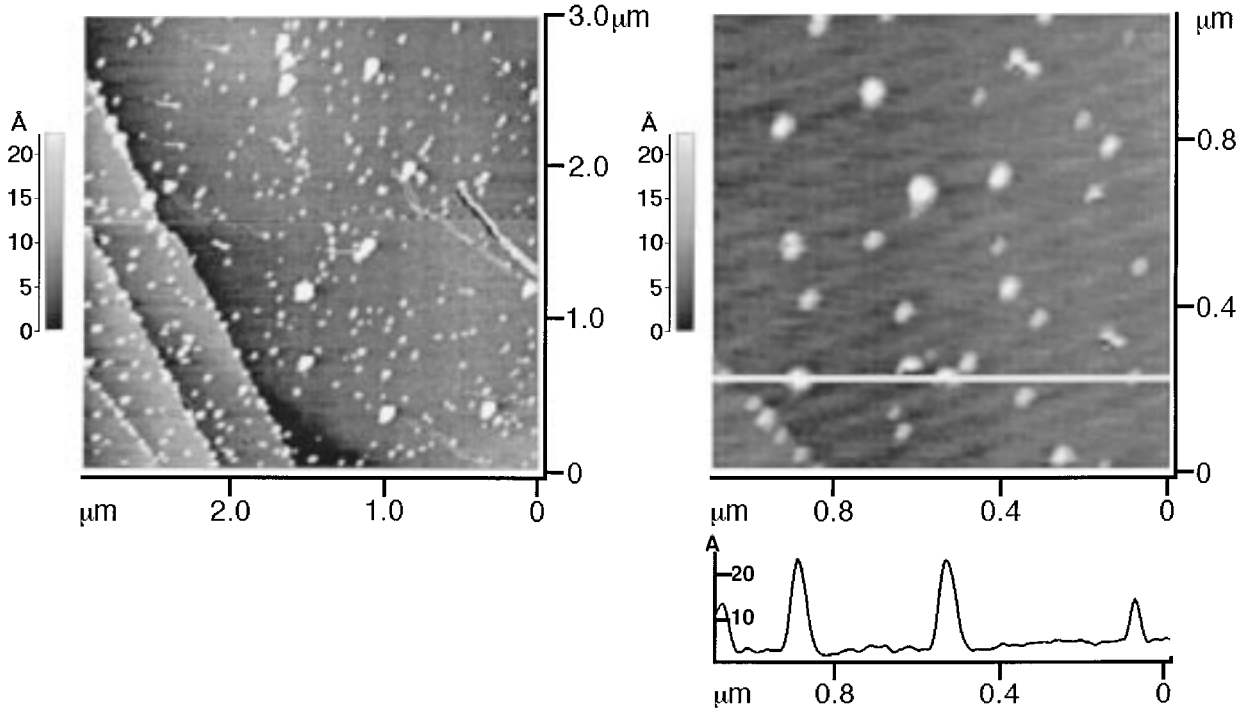


**Figure 2.** Noncontact atomic force micrographs of ZnO nanoparticles prepared using method 2 with a deposition time of 15 s. An amplitude trace corresponding to the location of the white line is shown for the 1.0 × 1.0 $\mu$m image at right.

and used temperatures in the range 25−85 °C. Two sets of deposition conditions have been sampled for this deposition method (our methods 2 and 3, above): Method 2 departs from the conditions employed by Peulon and Lincot only in the use of a slightly lower $Zn^{2+}$ concentration (1 vs 5 mM) whereas in method 3 $ClO_4^-$ has been substituted for $Cl^-$ in the deposition solution. The deposition potential in both cases was −0.04 V vs NHE, and, as shown in the Pourbaix diagram of Figure 1, this potential lies well negative of line "a" which marks $E^{\circ\prime}$ (∼+0.8V vs NHE) for reaction 5 in 1.0 mM $Zn^{2+}$.

From the standpoint of the topography of the deposit and its structure as determined using selected area electron diffraction, the ZnO particles and films prepared using methods 1−3 were remarkably similar. These characteristics are summarized in the following paragraphs.

Noncontact atomic force microscopy (NC-AFM) investigation of ZnO particles prepared using these methods revealed these deposits to be very heterogeneous in terms of the particle size and shape. The topography of a typical direct ZnO sample—this one prepared using the procedure of method 2 with a deposition time of 15 s—is shown in the two NC-AFM images of Figure 2. In these images, large (height > 50 Å) ZnO particles coexist on the graphite surface with smaller (height ≈ 20 Å) ZnO particles. In our previous investigations of metal and semiconductor nanocrystals,[31,32,34] we have noted that the AFM-measured nanoparticle height is, in fact, an excellent approximation to the TEM measured particle *radius*. Particle height histograms for ZnO particles prepared by any of the direct methods, such as those of Figure 2 obtained for ZnO particles prepared again using method 2, showed relative standard deviations of 40−50%. The distribution and areal density of particles (∼$10^9$ $cm^{-2}$) on the graphite surface are similar to what has been seen previously for silver,[34] platinum,[33] copper,[31] and cadmium[32] deposited at submonolayer coverages: First, the nucleation density on step edges approaches saturation (i.e., nuclei appear in AFM images to contact neighboring nuclei), whereas that on terraces is between 1 × $10^9$ and 5 × $10^9$ $cm^{-2}$. The relatively broad particle size distributions obtained for ZnO, however, contrast with the much narrower distributions which have been obtained for metal nanocrystallites grown on the graphite basal plane.[31,33,34] The implication is that the mechanism of nucleation and growth operating here is different from the instantaneous nucleation and diffusion-limited growth mechanism which is seen for metal nanocrytallite growth on the HOPG basal plane.[33,34]

Second, it was not possible to exercise control of the mean ZnO particle size in these experiments using the deposition time. For example, the three histograms of Figure 3 were compiled from NC-AFM height measurements for ZnO nanoparticles obtained using method 2. Although the deposition times ranged from 7 s (A) to 30 s (C) in these three experiments, a mean particle height in the range 13−17 Å was nevertheless obtained in each case. One obvious explanation for this outcome is that the electrochemical growth of ZnO to a height of ∼15 Å occurs relatively quickly, but growth from this point occurs at a slower rate because of the very low conductivity of ZnO. Much thicker ZnO films of up to ∼0.5 $\mu$m were prepared by depositing for periods of up to 1 h; however, a good correlation between the deposition time and the structure of the deposit could not be established for these long deposition times.

Selected area electron diffraction (SAED) measurements were employed to identify the deposited particles in these experiments and to determine the crystal

(34) Zoval, J. V.; Stiger, R.; Biernacki, P. R.; Penner, R. M. *J. Phys. Chem.* **1996**, *100*, 837.

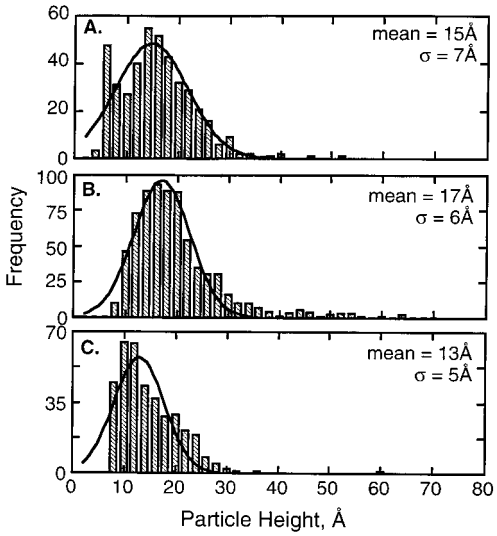


**Figure 3.** Histograms of ZnO nanoparticle heights measured using NC-AFM data. These samples were prepared using method 2 and deposition times of (A) 7, (B) 15, and (C) 30 s.

structure and the orientation of these particles on the graphite surface. In each of the three SAED patterns shown in Figure 4, several of the most prominent diffraction rings have been labeled as markers, and other diffractions can be identified by consulting the schematic SAED powder pattern for wurtzite phase ZnO shown in Figure 5. In Figure 4a is shown a SAED pattern for a chemically synthesized ZnO powder reference sample which, following its synthesis, was mechanically dispersed directly onto a carbon-coated gold TEM grid. Because of the method of preparation, the large ZnO particles of this reference sample possessed no preferred orientation with respect to the surface of the TEM grid, and all of the diffractions indicated in Figure 5 should be seen in the SAED pattern of Figure 4a. Indeed, this is the case except for two groups (the first [112] and [200]; the second [100], [002], and [101]) which were too close to one another to be completely resolved. In Figure 4b is shown a SAED pattern for a ZnO sample prepared using method 3. A comparison with the SAED pattern of Figure 5 reveals that those diffractions marked in that figure with a star are not observed. These diffractions are those deriving from periodicities in the wurtzite lattice existing along the *c*-axis of the crystal, and the extinction of these diffractions in the data of Figure 4b means that, on average, the wurtzite lattice of ZnO nanocrystals is oriented with the *c*-axis perpendicular to the plane of the graphite surface. Exactly the same diffraction pattern is seen for ZnO nanocrystals prepared using the E/C method (Figure 4c), and some further interpretation of these data can be found below. Qualitatively identical results were obtained for ZnO thin films prepared using methods 1 and 2, and it is therefore established that oriented, wurtzite phase ZnO is generated by all three of these procedures.

Of particular interest in this work are the luminescence characteristics of the ZnO particles and films prepared by methods 1−3. However, in this paper we have examined only luminescence from ZnO *films* since the blue-shifted absorption of ZnO particles could not be excited using the 3.5 eV (i.e., 351 nm) line of our $Ar^+$ laser. As mentioned earlier, luminescence spectra for ZnO have typically exhibited two peaks: an exciton band at 3.2 eV (387 nm) which derives from charge-transfer excitations of the type

$$Zn^{2+}-O^{2-} \rightleftharpoons [Zn^{+}-O^{-}]^* \qquad (6)$$

and, as already noted, a defect state emission which peaks in the range 1.95−2.75 eV (450−635 nm). Room temperature luminescence spectra for thin films (100 Å to 5.0 $\mu$m in thickness) of ZnO prepared using method 2 (cathodic electrodeposition from a chloride-containing electrolyte) reproducibly yielded spectra like that of Figure 6A. These spectra consisted only of a broad trap state emission; no exciton emission was seen for these samples. Remarkably, no systematic differences in these PL spectra were observed as a function of the film thickness over the range from 100 Å to 5.0 $\mu$m. This trap state emission has been reported in all previous spectroscopic investigations of ZnO nanoparticles and thin films and has even been a prominent feature of the emission spectra of micrometer scale ZnO powders[29] and macroscopic ZnO single crystals.[35] ZnO films prepared by cathodic electrodeposition using either methods 1 or 3 typically showed both trap state and exciton bands. In terms of the prominence of the exciton band relative to that of the trap state transition (characterized by $R_{295}$ (vide supra)), the best results were obtained for films prepared using method 3. Of the over 20 samples prepared ranging in thickness from 10 nm to 1.0 $\mu$m, the best spectrum seen is that shown in Figure 6B: Two spectra are shown for a film before, and following, annealing at 300 K in $O_2$ for 30 min. The intensity of the trap state peak was unaffected by annealing; however, the intensity of the exciton emission band increased substantially with the consequence that $R_{295}$ improved from 1.2 to 0.25 in this experiment. The $R_{295}$ value seen for annealed films prepared using method 3 is within 0.10−0.20 of the lowest reported previously in the literature. If is important to note that methods 2 and 3 are identical except for the substitution of $ClO_4^-$ for $Cl^-$ in method 3. Thus, dramatically improved emission characteristics for ZnO films prepared using the Peulon and Lincot method is obtained simply by eliminating $Cl^-$ from the synthesis solution.

**III.B. ZnO Prepared by the Electrochemical/Chemical Method.** The E/C synthesis of ZnO particles or films (depicted schematically in Scheme 1B) was carried out by first electrochemically depositing zinc metal from a perchloric acid electrolyte at a potential of −1.1 V vs NHE. Once the deposition step was complete (in 100 ms to 30 s), the electrode was permitted to equilibrate with the plating solution at open circuit for a few seconds and the oxidation of the zinc deposit proceeded concurrently with the evolution of hydrogen on these particles. As shown in the Pourbaix diagram of Figure 1, this corrosion reaction is driven by ∼1.0 V of thermodynamic driving force. In the following paragraphs, we describe the properties of the particles and thin films obtained using this two-step method.

Noncontact AFM images of E/C-synthesized ZnO nanocrystallites look qualitatively similar to those for "direct" ZnO because particles are distributed in a

(35) Idriss, H.; Andrews, R. M.; Barteau, M. A. *J. Vac. Sci. Technol. A* **1993**, *11*, 209−18.

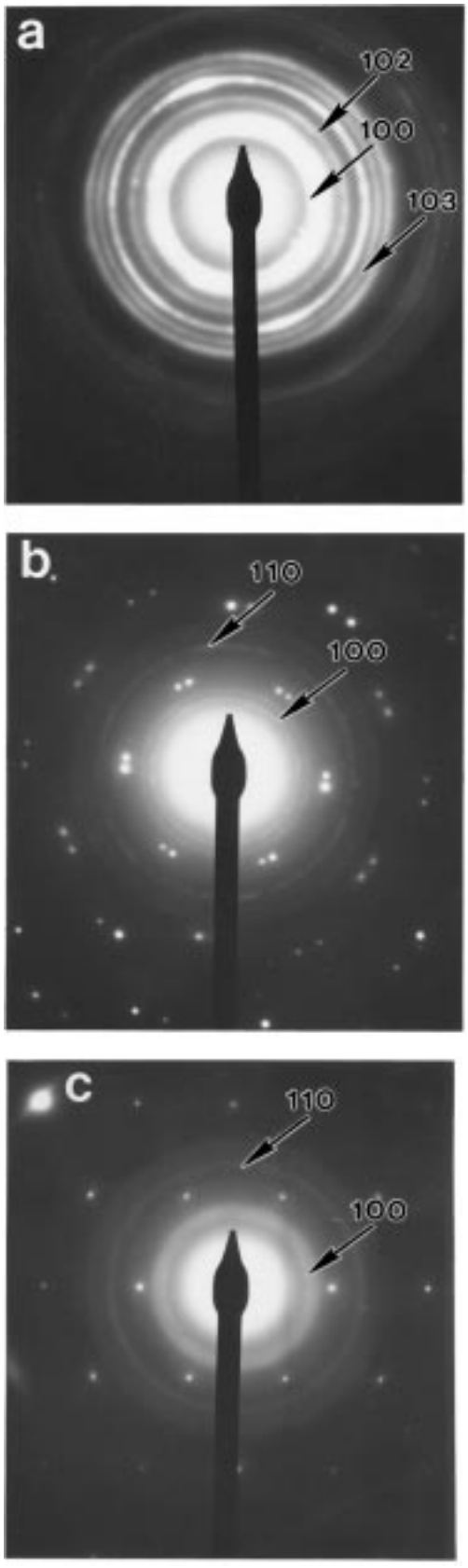


**Figure 4.** Selected area electron diffraction data for ZnO particles prepared as follows: (a) chemically synthesized ZnO powder dispersed on HOPG, (b) ZnO nanoparticles prepared using method 2 and a deposition time of 15 s, and (c) ZnO nanoparticles prepared using the E/C method and a deposition time of 1.0 s.

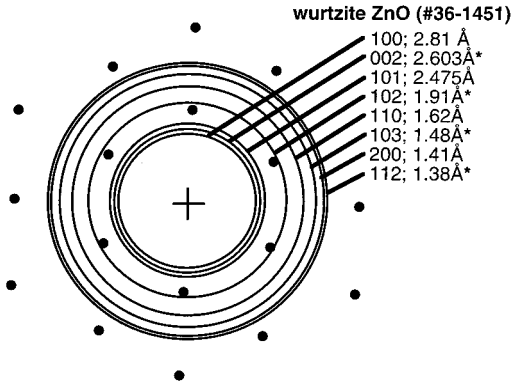


**Figure 5.** Schematic diagram of the SAED pattern expected for wurtzite phase ZnO (X-ray powder diffraction file #36-1451). The indices labeled with stars were not observed in the SAED patterns of ZnO nanoparticles prepared using methods 1−3 or the E/C method.

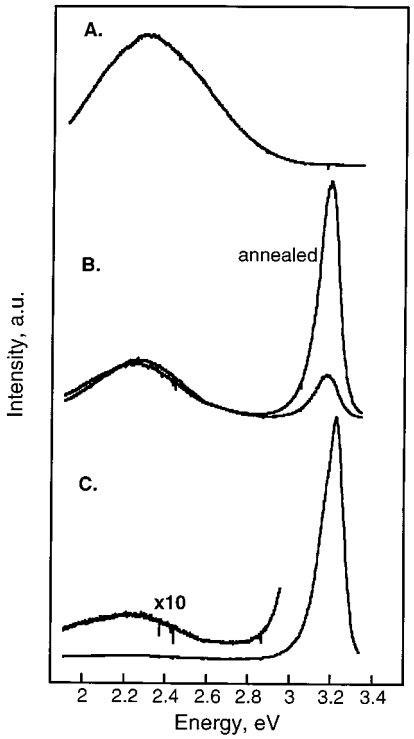


**Figure 6.** Luminescence spectra for ZnO films: (A) method 2; deposition time = 20 min, annealed 10 h at 300 K, integration time = 0.10 s at $T = 20$ K. This film possessed a thickness of 1−5 $\mu$m; (B) method 3; deposition time 15 min, annealed 10 h at 300 K, integration time = 5 s at $T = 295$ K (this film possessed a thickness of ∼1 $\mu$m); (C) E/C deposited for 30s, integration time = 0.05 s at $T = 295$ K (this film possessed a thickness of ∼10 nm). For all three spectra, excitation energy = 3.53 eV; laser fluence ≈ 50 mW.

similar way on the graphite surface. Shown in Figures 7, 8, and 9 are NC-AFM data for surfaces prepared using zinc deposition pulses having durations of 50 ms, 0.5 s, and 1.0 s, respectively. In Figure 8, ZnO particles can be seen to nucleate in dense "lines" in the graphite surface. These lines, which have also been seen in our previous work with silver and platinum, often do not correspond to step edges on the graphite surface and may instead represent the positions of subsurface grain boundaries or steps. Terraces are again decorated with ZnO particles at a coverage of $(1-5) \times 10^9$ cm$^{-2}$. In Figure 7, which shows ZnO particles having a mean

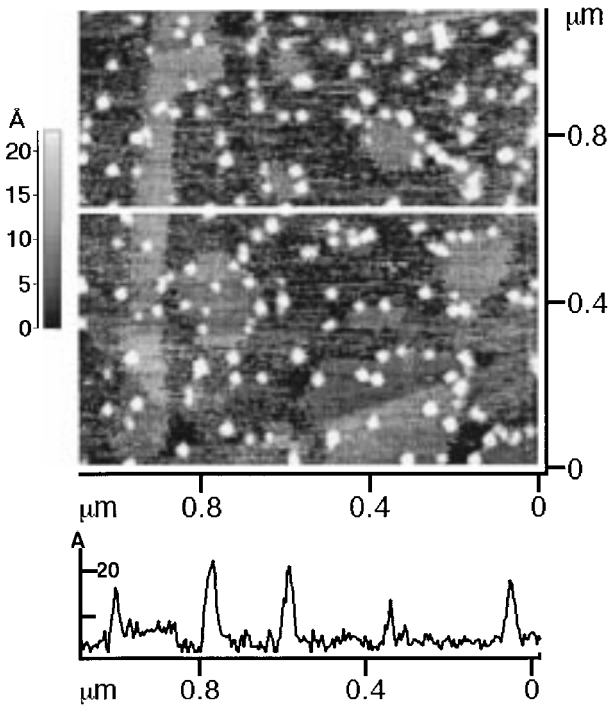


**Figure 7.** Noncontact atomic force micrograph of ZnO nanoparticles prepared using the E/C method with a deposition time of 50 ms. An amplitude trace corresponding to the location of the white line is shown.

height of just 12 Å, a hydration layer—visible as gray islands 4−6 Å in height—is also visible on the graphite surface. This layer, which we have seen occasionally in the past, is fluxional from image to image and its spatial extent depends qualitatively on the ambient humidity. In areas of the surface where this layer was observed, particle heights were, of course, measured relative to nonhydrated regions of the surface.

Histograms of ZnO particle heights compiled from NC-AFM images are shown in Figure 10. As can be seen here, relative to the ZnO particles prepared by any of the three "direct" deposition methods, the height distributions for the particles obtained by E/C were narrower. This difference was particularly pronounced for samples having "small" ZnO nanocrystallite (mean height < 20 Å) particles where standard deviations as low as 3−4 Å were obtained. These narrow distributions imply that the nucleation of zinc on the graphite surfaces is instantaneous, just as previously seen for the deposition of silver, copper, cadmium, and platinum. Clear electrochemical evidence for instantaneous nucleation, however, is not available because hydrogen evolution obscures the zinc deposition current in these experiments. Control of the mean particle size using the zinc plating pulse duration was also possible—again in contrast to the case with methods 1−3 and again in analogy to previous work with other metals. In fact, over the range 1−3 s, an approximately linear increase in the ZnO particle height to 60 Å was seen in data pooled from 20 experiments, as shown in the plot of Figure 11. Beyond 3s, the growth of the ZnO deposit accelerates, and particles on the surface merge to form a layer the height of which increases more rapidly with time. This acceleration in the ZnO growth rate is attributed to the secondary nucleation of zinc metal on top of "primary" zinc nanocrystallites in the first step of the synthesis—where "primary" zinc particles are defined as those that nucleated directly on the graphite surface. As shown below, the orientation of these secondary ZnO particles is not correlated with that of primary ZnO particles.

As already noted above, the SAED data for ZnO nanoparticles prepared by E/C were indistinguishable from that for "direct" ZnO particles: E/C ZnO particles were wurtzite phase, and diffractions from periodicities

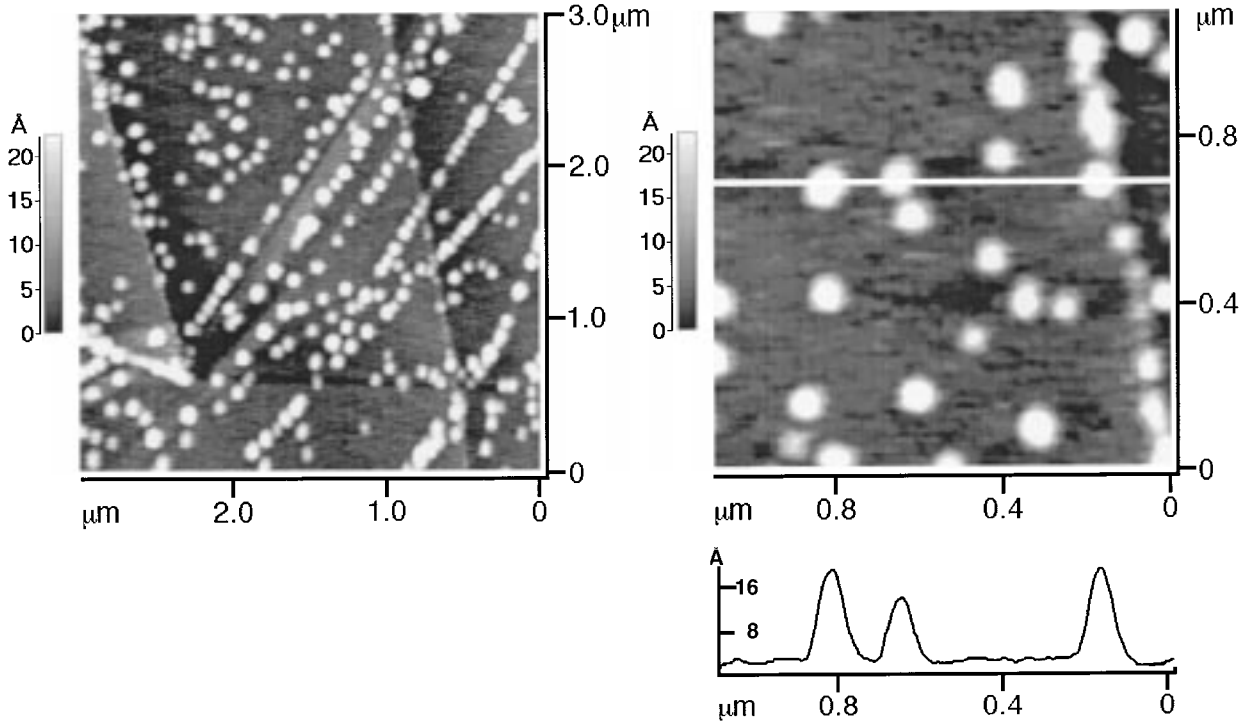


**Figure 8.** Noncontact atomic force micrographs of ZnO nanoparticles prepared using the E/C method with a deposition time of 1 s. An amplitude trace corresponding to the location of the white line is shown for the 1.0 × 10 $\mu$m image at right.

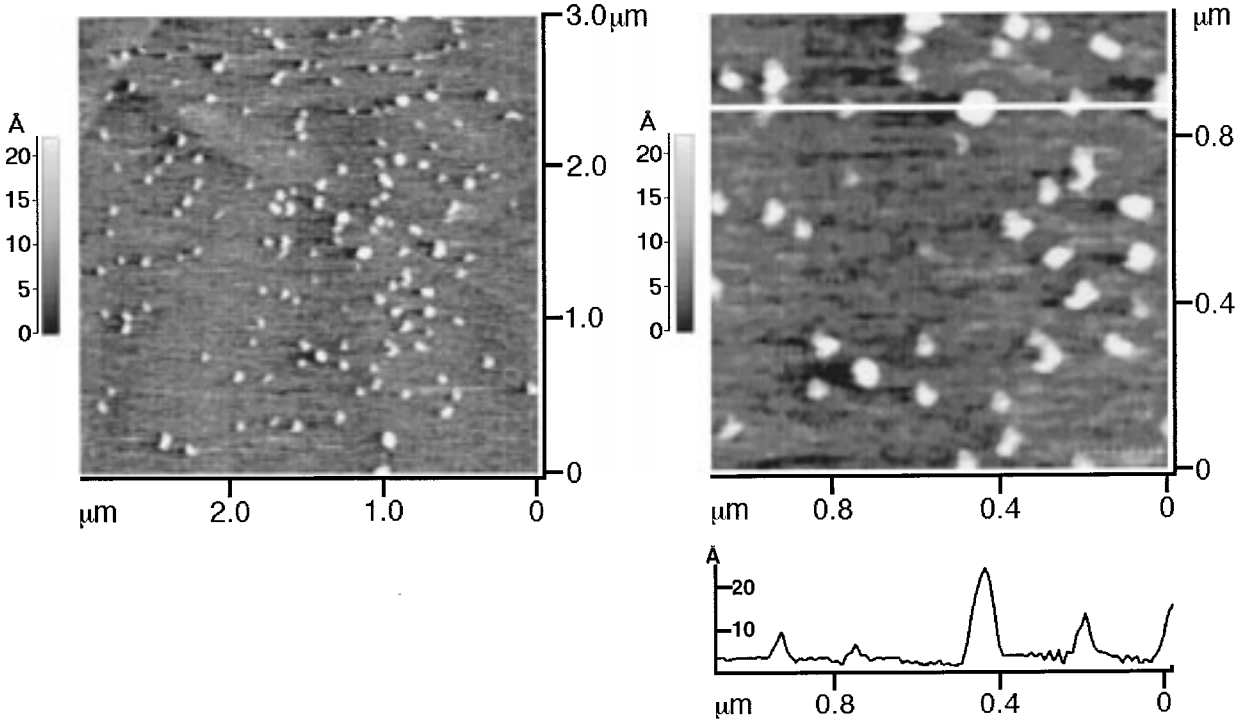


**Figure 9.** Noncontact atomic force micrographs of ZnO nanoparticles prepared using the E/C method with a deposition time of 3 s. An amplitude trace corresponding to the location of the white line is shown for the 1.0 × 1.0 $\mu$m image at right.

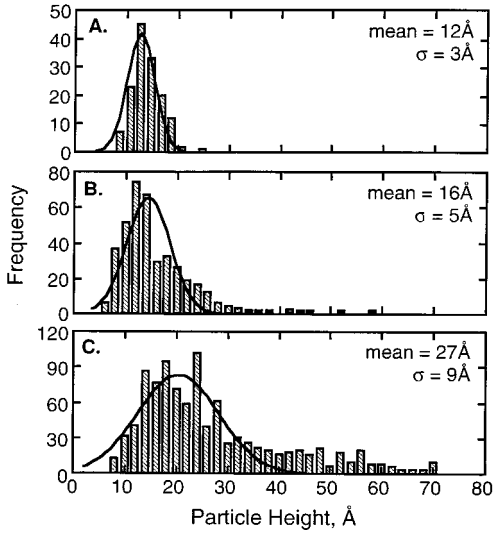


**Figure 10.** Histograms of particle heights for E/C-synthesized ZnO nanocrystallites measured using NC-AFM. Deposition times were (A) 50 ms, (B) 1.0 s, and (C) 3.0 s.

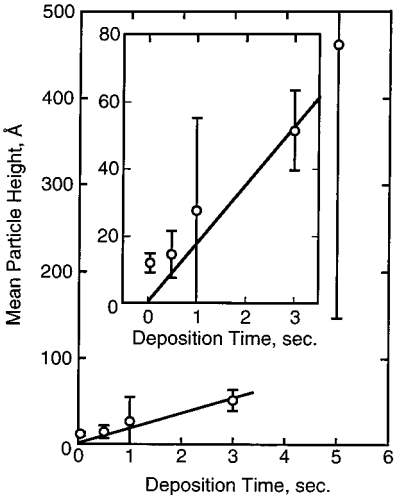


**Figure 11.** Plot of the mean ZnO particle height (measured using NC-AFM) vs the zinc deposition time. Data from two–three samples were averaged to generate the height statistics (mean and standard deviation) at each time.

along the *c*-axis (starred indices in Figure 5) were missing from the pattern, indicating that a preference exists for a crystallite orientation in which the *c*-axis is oriented perpendicular to the plane of the graphite surface. In previous work involving the E/C synthesis of wurtzite phase CuI[31] and CdS[32] nanocrystals, epitaxial alignments of both types of particles on graphite was seen by SAED. That epitaxial ZnO nanocrystals are not obtained is easily rationalized in the context of the calculation shown in Figure 12. In this figure is plotted the total energy of a rigid island (composed of ZnO, CdS, or CuI) containing 126 atoms in two layers. For a particular angular orientation of the island on a rigid graphite surface (containing 1882 atoms in two layers), the island energy was calculated as a function of distance from the surface by summing the pairwise interactions of each atom in the island with each atom in the surface. The pairwise potential describing these interactions was a generic Lennard-Jones (L-J) potential with well depth $\epsilon_o$, and $\sigma = 3.0$ Å (where $\sigma$ is the value of $r$ at which $V(r) = 0$). Since the parametrization of the L–J potential has not been established for any of the three materials of interest, the relative energy, $E/\epsilon_o$, has been plotted instead of an absolute energy in Figure 12. This fact does not diminish the utility of this calculation since it is the *relative preference* of an island for a particular angular orientation which we seek to determine. A prominent minimum in the energy at 30° for both CuI and CdS is seen in Figure 12, which corresponds to a coincidence of these lattices with the

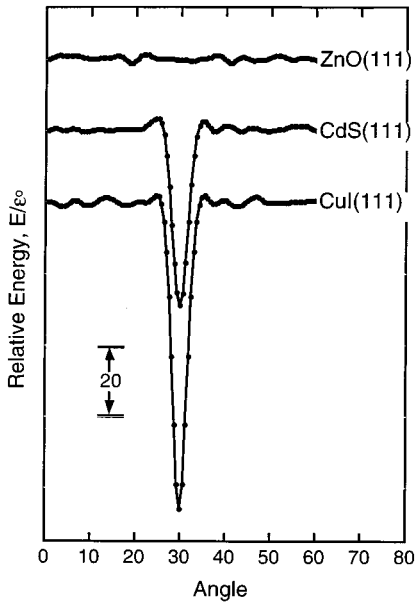


**Figure 12.** Normalized energy, $E/\epsilon°$, of two-layer thick semiconductor islands on a two-layer thick graphite surface calculated using Lennard-Jones potentials having a well-depth, $\epsilon°$, located at $\sigma = 2.0$ Å. Each island was approximately 25 Å in size and consisted of 126 atoms; the graphite surface consisted of a total of 1882 atoms.

hexagonal graphite surface. The orientation of the CuI and CdS islands at this minimum is the same as that which has been seen[31,32] in the SAED data for these two materials. A similar energetic minimum is obviously missing from the ZnO calculation, and this provides an immediate justification for the absence of in-plane alignment of the ZnO unit cell on graphite.

Surprisingly, even in comparison with the ZnO films prepared by method 3 (e.g., spectrum 4b), superior luminescence spectra—exhibiting no trap state emission at room temperature—were obtained for ZnO films prepared using the E/C approach. This result was robust in terms of the range of Zn° deposition times which were explored, ranging from 2 (corresponding to a dense collection of 80−100 Å nanoparticles) to 30 s (corresponding to semicontinuous ZnO films with thickness near 400 Å). For E/C ZnO particles smaller than ~60 Å, no fluorescence emission could be detected because the quantum size effect-induced blue-shifted emission from these particles is not excited by the 351 nm $Ar^+$ line used in this work. Emission from quantum-confined ZnO nanoparticles, excited with light of higher energy, will be the subject of a future publication. A typical emission spectrum for a ZnO film prepared by E/C is shown in Figure 6C. In this spectrum, the trap state "peak" has an a maximum amplitude (at 2.34 eV) of 45 counts while the exciton emission band peaks at 5900 counts for the ratio $R_{295} = 0.008$. The luminescence of these samples was stable in the laboratory air ambient for periods of at least 48 h following preparation.

At lower temperatures, the intensity of the green emission from ZnO is known to decrease relative to the exciton band, cf. 16, and a slight increase in the band

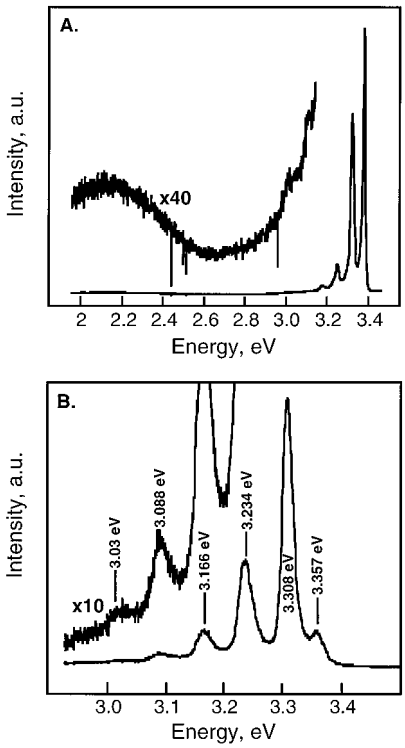


**Figure 13.** Low-temperature (20 K) luminescence spectra for an E/C-synthesized ZnO film (~10 nm in thickness) deposited for 30 s on HOPG: (A) low-resolution spectrum, (B) high-resolution spectrum.

**Table 1. Comparison of Exciton Emission Peak Positions for E/C-Synthesized ZnO with Theoretical Predictions[36]**

| expt peak energy (eV) | theor peak energy[36] (eV) | assignment |
|---|---|---|
| 3.357 | 3.360 | bound exciton |
| 3.308 | 3.310 | free exciton−LO |
| 3.234 | 3.238 | −2LO |
| 3.166 | 3.162 | −3LO |
| 3.088 | n.a. | −4LO |
| 3.03 | n.a. | −5LO |

gap (by ~157 meV at 20 K) is seen as a consequence of the contraction of the ZnO unit cell. Phonon excitations of these nanocrystals are not supported at this temperature and the exciton peak becomes split into a series of lines which are separated from the zero phonon line by spacings which are close to multiples of the longitudinal optical phonon energy (LO, 2LO, 3LO, etc) of ~600 $cm^{-1}$. In addition to this phonon loss progression, a bound exciton emission peak at slightly higher energies has sometimes been observed.[16] All of these effects are manifested in the luminescence spectrum of Figure 13A for an E/C-synthesized ZnO film which was acquired at 20 K. In this spectrum, the green emission at 2.1−2.2 eV is barely detectable above background, and the exciton line exhibits a fine structure; the details of which are revealed in the high-resolution spectrum of Figure 13B. Each of the lines seen in this envelope can be assigned with confidence since an excellent correlation with theoretical predictions for ZnO[36,37] exists. These assignments and a comparison with Klingshirn's[37] theoretical predictions are shown in Table 1. The free-exciton-1LO peak has usually exhibited the greatest intensity, and in conjunction with the excellent agreement seen with theory, this band "anchors" the assignment of the others in the spectrum. Theoretical pre-

(36) Klingshirn, C.; Levy, R.; Frun, J. B.; Honerlage, B. *Sol. Stat. Comm.* **1976**, *20*, 413−17.
(37) Klingshirn, C. *Phys. Stat. Sol. B* **1975**, *71*, 547−56.

dictions for the −4LO and −5LO energies are missing from this table presumably because these lines have not been seen clearly in any previous data to our knowledge, and no motivation therefore has existed for a theoretical analysis of these transitions until now. The exceptional quality of this low-temperature emission spectrum provides another indication that the defect content of our E/C-synthesized material is extremely low.

## IV. Summary

Wurtzite phase ZnO particles and thin films have been synthesized using a new electrochemical/chemical procedure. This E/C method possesses the following characteristics: (1) ZnO nanoparticles are narrowly dispersed in size—particularly for particle dispersions have mean diameters smaller than 20 Å; (2) The mean ZnO particle size is adjustible via the $Zn^0$ deposition duration; (3) Particle areal densities of $10^9-10^{10}$ $cm^{-2}$ are obtained, however, ZnO particles remain well separated from one another on average, (4) ZnO nanoparticles possess a preferred orientation on the graphite surface (*c*-axis perpendicular to the surface), however, ZnO films do not; (5) Pure exciton emission is seen in the luminescence spectra for ZnO films.

A chemical or structural basis for the remarkably clean emission spectra seen for E/C-synthesized ZnO has not been pinpointed in this study and it is hoped that more detailed investigation of these particles by surface vibrational spectroscopic methods will yield information on the termination of the ZnO surfaces of direct and E/C-synthesized material. However the luminescence spectra for E/C ZnO do show unequivocally that the defect states responsible for the "green" trap state emission seen in all previous experiments cannot be intrinsic to ZnO.

**Acknowledgment.** The financial support of this work was provided by a grant from the Office of Naval Research (#400X119YIP). R.M.P. also acknowledges financial support as a National Science Foundation Young Investigator (#DMR-9257000), an A.P. Sloan Foundation Fellow, a Camille Dreyfus Teacher-Scholar, and an Arnold and Mabel Beckman Foundation Young Investigator. S.G. acknowledges the financial support of a Welch Scholarship of the International Union for Vacuum Science. G.E. thanks the Deutsche Forschungsgemeinschaft for financial support. The authors express their gratitude to Dr. Art Moore of Advanced Ceramics Inc. for the donation of some of the graphite employed for these investigations.

CM970718M